

Optics Letters

Telecentric suppression of diffuse light in imaging of highly anisotropic scattering media

MICHELLE A. VISBAL ONUFRAK,¹ RAYMOND L. KONGER,² AND YOUNG L. KIM^{1,3,*}

¹Weldon School of Biomedical Engineering, Purdue University, West Lafayette, Indiana 47904, USA

²Department of Pathology & Laboratory Medicine and Department of Dermatology, Indiana University School of Medicine, Indianapolis, Indiana 46202, USA

³Department of Computer Science and Engineering, Kyung Hee University, Yongin 17104, South Korea

*Corresponding author: youngkim@purdue.edu

Received 20 November 2015; accepted 21 November 2015; posted 25 November 2015 (Doc. ID 254317); published 22 December 2015

The telecentric lens, which was originally used in the machine vision industry, has often been utilized in biomedical imaging systems due to its commonly known properties, such as large transverse field of view, constant magnification, and long working distance. However, its potential advantages in optical imaging of biological tissue, which is highly diffusive, have not been fully explored. We revisit the idea that a telecentric lens system can bring an alternative yet simple method for reducing unwanted scattering or diffuse light in biological tissue, owing to its highly anisotropic scattering properties. Using biological tissue and tissue phantoms, we demonstrate advantages attributed to the use of telecentric lens in tissue imaging compared with imaging using conventional nontelecentric optics. Directional or angular gating (or filtering) using a telecentric lens is beneficial for removing a portion of diffuse light in highly anisotropic scattering media with high values of the scattering anisotropy factor. We envision that a telecentric lens could be potentially incorporated into an instrument of modest design and cost, increasing rapid practical adoption. © 2015 Optical Society of America

OCIS codes: (290.4210) Multiple scattering; (160.1190) Anisotropic optical materials; (170.3660) Light propagation in tissues; (170.0110) Imaging systems; (170.3890) Medical optics instrumentation.

<http://dx.doi.org/10.1364/OL.41.000143>

Light propagation in biological tissue is of a highly diffusive nature, as it encounters multiple scattering events. This scattered diffuse light is responsible for often masking an object embedded in the biological scattering medium, hence losing most of the image information on the object of interest. To isolate ballistic and snake-like light, a variety of optical imaging technologies, including confocal microscopy and optical coherence tomography, have been successfully developed as the holy grail of biomedical optical imaging. Indeed, such advanced imaging systems are already translated into the current clinical practice. On the other hand, there is still a need for simple and cost-effective imaging systems for overcoming the

limitation of tissue imaging, which could potentially be integrated with smartphones or be used for home-based care in resource-limited settings. Thus a simple yet effective method for removing diffuse light in planar tissue imaging would be beneficial, even with slightly inferior performance compared with the aforementioned advanced systems.

As an alternative approach, diffuse light can also be relatively suppressed using directional (or angular) gating (or filtering) in the detection arm, because the diffuse light component travels the medium deviating from the incident angle of illumination [1]. In a transmission mode (i.e., forward scattering) in turbid media, a small acceptance angle can reduce the number of scattering events [2]. In tissue optics, this optical property is characterized by the scattering anisotropy factor $g = \langle \cos \theta \rangle$, where θ is the scattering angle in the forward direction. It is well known that most biological tissue has a high value of $g \sim 0.8\text{--}0.95$, which means a high directional tendency of scattered light with respect to the incident direction (i.e., highly forward scattering) [3,4]. The detailed mechanism of optical clearing agents (e.g., glycerin and DMSO) for tissue imaging has been elucidated by quantifying variations in g [5]. In particular, commonly used clearing agents significantly increased g with minimal changes in the scattering coefficient in skin tissue. The highly anisotropic light propagation in biological tissue can also provide additional benefit to directional gating [6–8]. Under directional gating in the backward direction, which collects a small solid angle ($\theta < 2^\circ$) in a reflection imaging mode, the intensity at each pixel or location can be mainly determined by g of the tissue being imaged, allowing for an intrinsic image contrast weighted by g [8].

In this respect, we revisit the use of telecentric lens systems that are often used in wide-field optical imaging systems, due to the apparent advantages (e.g., large field of view, constant magnification, reduced aberration, and long working distance). We introduce that a telecentric lens can provide a simple mesoscopic (between microscopic and macroscopic) imaging platform for removing diffuse light in tissue imaging. A telecentric lens is a compound lens system modified with an additional aperture, which provides for achieving constant magnification and focus over a long distance. Telecentric lenses can remove the parallax error that makes closer objects appear

to be larger than objects farther from the lens [9]. Although telecentric lenses have been primarily used in the manufacturing industry, integrated into machine vision systems for defect recognition during assembly lines and package inspections, they have also been adopted into optical computed (or emission) tomography and the reference scanning arm of optical coherence tomography [10–13]. For instance, in optical computed tomography, a telecentric lens with a small acceptance angle of $\sim 0.1^\circ$ has been used to remove stray light in transmission mode, which is analogous to antiscatter grids for x rays or γ rays [13]. Implementation of a telecentric lens into optical coherence tomography has proven ideal for clinical situations where the flat image provided by the telecentric optics can overcome the curvature or distortion of the objective of interest [14–16]. In a similar manner, telecentric lenses have recently been used in digital holographic microscopy for curvature phase correction [17]. Still, the possible advantage of using telecentric lenses has not yet been explored systematically when combined with imaging of highly anisotropic scattering media, specifically biological tissue.

In this Letter, we take advantage of a telecentric lens system to easily implement directional angular gating in a reflection mode of optical tissue imaging, which can discard a relatively significant amount of unwanted scattered or diffuse light in highly anisotropic biological tissue. In our study, we intend to explore the dependence of the scattering properties of biological tissues, in particular $g = \langle \cos \theta \rangle$, for diffusion suppression using a telecentric lens. First, we characterize the telecentricity (i.e., acceptance angle for image formation) of a telecentric lens that allows for large-area tissue image with demagnification (e.g., $0.3\times - 0.2\times$). Second, we evaluate possible variations in system configurations by employing a telecentric lens or a conventional nontelecentric lens, in conjunction with two different types of illumination: collimated (or directional) light illumination and diffuse light illumination. Third, using mouse skin tissue as an anisotropic scattering medium, we compare resolving power of a target object placed underneath the skin to assess diffuse light removal. Finally, we conduct a series of tissue phantoms to better understand the role of the scattering anisotropy factor in image resolution of objects deeply embedded in tissue-like scattering media under different system configurations.

First, we determined the degree of telecentricity of the telecentric lens (magnification of $0.3\times$, Schott Moritex Co.) that is capable of mesoscopic tissue imaging in a field of view of 50 mm in diameter, using a telecentricity target (Edmund Optics, Inc.). The degree of telecentricity refers to an acceptance angle in image formation over the field of view. When the flat surface of the telecentricity target was placed at 45° with respect to the optical axis [Fig. 1(A)], a nontelecentric lens [Fig. 1(B)] (magnification max $0.22\times$ and aperture diameter of $f/4$, Edmund Optics, Inc.) shows a decrease in magnification with distance between the object and the lens (also known as the keystone effect). On the other hand, the target image of the telecentric lens clearly depicts the straight vertical lines with no size or perspective angle changes [Fig. 1(C)]. For the telecentric lens, the telecentric angle (i.e., acceptance angle), defined by the angle between the tilted line profile and the vertical line, was 0.55° , whereas the conventional lens had an average angle of 5.52° . In particular, our hypothesis is that, having such a small acceptance angle, the telecentric lens can

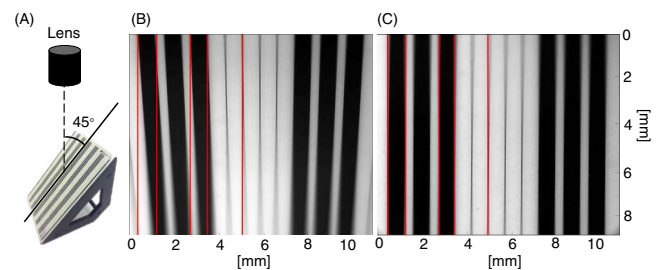


Fig. 1. Demonstration of telecentricity and telecentric angle measurements. (A) Telecentricity target whose flat surface stands at 45° with respect to the optical axis. (B) and (C) Images of telecentricity target acquired using a conventional nontelecentric lens and a telecentric lens, respectively. Vertical red guide lines added to show telecentric angles.

remove off-axis, unwanted diffuse light in a reflectance mode, when the surface of biological tissue is imaged in a planar manner. In other words, because the exit angle of the light diffused from biological tissue at the tissue surface is large, the telecentric lens can act as back-directional angular gating for simply discarding a portion of off-axis, unwanted diffuse light in the highly anisotropic scattering medium.

To implement the telecentric lens for reflectance imaging of tissue and compare it with conventional nontelecentric imaging, we built mesoscopic-imaging systems employing a telecentric lens or a conventional lens. We also tested two different types of illumination: collimated or directional light via a coaxial illumination port (A) and diffuse light via a ring illuminator (B). This also allowed us to investigate the need for collimated light via coaxial illumination (also known as inline telecentric lenses) to exploit the telecentric lens in the detection. As a result, three different configurations of illumination and detection pairs were constructed as shown in Fig. 2. A 75 W Xenon lamp with a bandpass filter at 550 nm was used as a light source. This beam was coupled to the telecentric lens to provide for either coaxial illumination (A) or to a ring illuminator (B) onto the sample via a fiber optic light guide. The light reflected from the sample was acquired using the same telecentric lens mounted with a CCD camera (Princeton Instruments, Inc.). When the illumination output beam was at a proper distance to achieve a focused image for either a telecentric

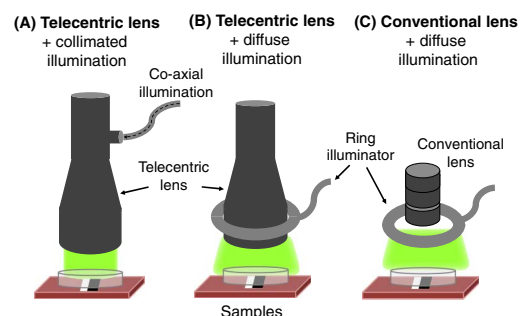


Fig. 2. System configurations by employing a telecentric lens or a conventional lens, in conjunction with two different types of illumination. (A) Telecentric imaging with a coaxial illuminator for collimated (or directional) light illumination. (B) Telecentric imaging with a ring illuminator for diffuse light illumination. (C) Conventional nontelecentric imaging with a ring illuminator for diffuse light illumination.

or conventional lens, the divergence angles of the illumination beam for both cases were $\sim 0.5^\circ$ and $\sim 0.9^\circ$ for the coaxial illuminator and the ring illuminator, respectively. For all of the systems, the field of view was $\sim 60 \text{ mm} \times 60 \text{ mm}$ with a pixel size of $\sim 77 \text{ }\mu\text{m}$. A minor nonuniformity of the illumination on the sample was also compensated by normalizing with a reference measurement from a white reflectance standard (WS).

Then, as representative biological tissue, we utilized SKH-1 hairless mouse skin [18] as scattering media with a black-and-white edge image placed underneath and attempted to resolve the black-and-white that was now embedded under the mouse skin, as shown in Fig. 3. In this case, where a target object is embedded in a scattering medium, the enhancement of the image resolution of the target provides direct information on how much unwanted diffuse light is removed. The scattering properties of the mouse skin tissue were determined using an integrating sphere method [18,19]: (i) scattering mean-free path length (i.e., averaged distance of a single scattering event) $l_S = 81.5 \pm 12.5$ (standard deviation) μm , (ii) anisotropy factor $g = 0.84 \pm 0.04$, and (iii) optical thickness $\tau = 12$ at 632 nm (physical thickness = $\tau \times l_S$). From grayscale images obtained from the three configurations, we characterized the resolving power of the edge target by computing image resolution using the knife-edge method [20]. An image area of 200 pixels ($\sim 15 \text{ mm}$) in height was selected from the grayscale image in Fig. 3(A), crossing horizontally between the black to the white areas of the edge and was averaged vertically, representing an edge spread function (ESF), as shown in Fig. 3. To compensate for speckle-like noise, ESF was fitted with a Fermi function such that

$$\text{ESF}(x) = \frac{a}{e^{((x-b)/c)} + 1} + d, \quad (1)$$

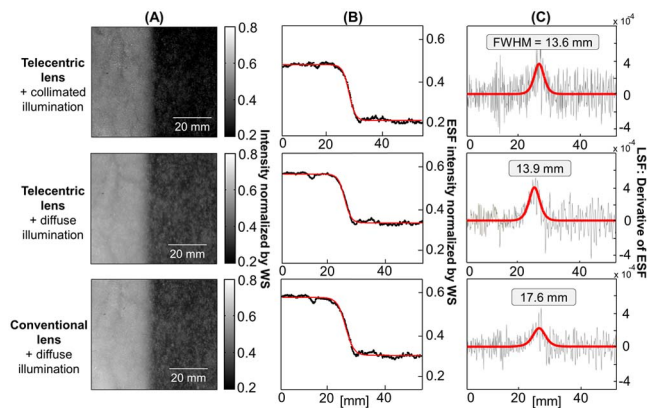


Fig. 3. Planar imaging of white-and-black edge targets embedded in biological tissue (hairless mouse skin) using three different system configurations. Note that the skin tissue is spatially heterogeneous in the large imaging area. (A) Grayscale images of the edge target underneath the mouse skin. Images are normalized by a reference image obtained from a WS. (B) Black line: averaged ESF of the edge target. Red line: ESF was fitted with a Fermi function to reduce noise-like signals from spatial nonuniformity of the skin, due to large-area imaging. (C) Calculated LSF, from the original averaged data (black) and the Fermi fit (red). FWHM is calculated to quantify the resolving power of the embedded target as an image resolution. Note that direct computations of LSF from the noise-like ESF curves drastically amplify intensity fluctuation in LSF, masking the critical information (i.e., FWHM in LSF).

where a , b , c , and d are constants. As shown in Fig. 3, we obtained a line-spread function (LSF) by taking the derivative of ESF with respect to x :

$$\text{LSF}(x) = \left| \frac{d \text{ESF}(x)}{dx} \right|. \quad (2)$$

Then, the resolving power of the edge target was calculated with a full width at half-maximum (FWHM) of LSF as an image resolution. Figure 3(C) reveals that both telecentric lens configurations have similar image resolution of 13.6 and 13.9 mm for the coaxial and ring illuminators, which are $\sim 25\%$ lower than that of the conventional nontelecentric lens system with a FWHM of 17.6 mm.

Next, we conducted a series of tissue phantoms to investigate the effect of g on the image resolution of an embedded target using telecentric imaging versus conventional imaging. In particular, we compared resolution enhancement resulting from diffuse light suppression as a function of g , while keeping other scattering properties (i.e., l_S and τ) fixed. First, we prepared four tissue phantoms with different g using aqueous suspensions of polystyrene microspheres (Polysciences Inc.) for $g = 0.51, 0.76, 0.85$, and 0.90 at $\lambda = 550 \text{ nm}$, while $l_S = 150 \text{ }\mu\text{m}$ and $\tau = 15$ were kept identical for each g . The scattering properties of the tissue phantoms were calculated using Mie theory [21,22]. The scattering media of $g = 0.85\text{--}0.90$ are considered to be close to most biological tissue, skin in particular [3,23]. Second, to carry out similar imaging tests, we replaced the mouse skin with different tissue phantoms prepared to mimic biological scattering media and placed them over a white-and-black edge image. For each g , at least six different tissue phantoms were prepared and imaging tests were repeated independently.

Figure 4 shows representative grayscale images for each tissue phantom using the three imaging configurations presented. Overall, as g increases, more clear distinctions between the white-and-black edge images are seen from telecentric imaging (A and B) due to the relative suppression of unwanted diffused light. On the other hand, the edge images are relatively invariable without strongly depending on g for conventional nontelecentric imaging (C). Similar to the analyses in the previous example using the mouse skin, we computed image resolutions for sample replicates with different g under the three system configurations. In Fig. 5, both telecentric imaging systems (A and B) show rapid decreases in FWHM of LSF (i.e., resolution enhancement) as g approaches to the typical values of biological tissue. However, the conventional nontelecentric system (C) in Fig. 5 is not dependent on g with no statistical significance (i.e., $p\text{-value} = 0.19$ for the slope between FWHM of LSF and g). In other words, only backscattered images acquired by the telecentric lens with either the coaxial or ring illuminators were sensitive to changes in g , in contrast to its conventional lens-imaging counterpart. These results support the idea of simple yet effective removal of a portion of diffuse light in biological tissue imaging using a telecentric lens.

In conclusion, we demonstrated the unique ability of telecentric lenses used in tissue imaging to remove a relative portion of unwanted scattered or diffuse light in highly anisotropic scattering media. Telecentric lens systems present an advantage of enhancing the resolving power of an embedded object through scattering media, such as mouse skin, owing to the

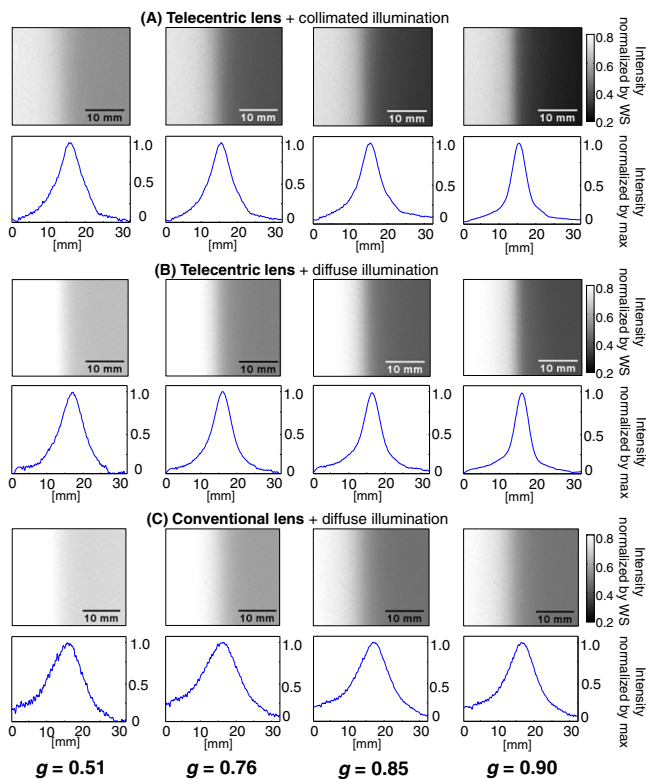


Fig. 4. Representative grayscale images of white-and-black edge targets embedded in tissue phantoms consisting of microsphere suspensions with four different g , using three different system configurations. Each corresponding LSF is included below the images. Note that the phantom studies do not require any fitting, because the relatively smooth images originated from the unique aqueous suspension of microspheres and the Brownian motion.

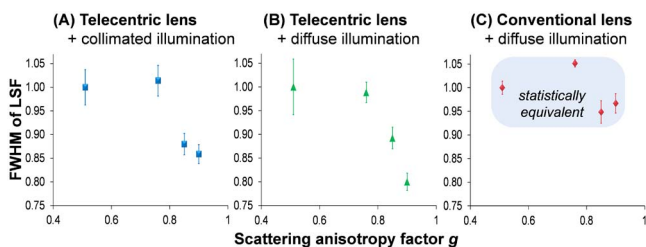


Fig. 5. Effect of g on the resolving power of an embedded target, using telecentric imaging versus conventional imaging. FWHM of LSF (i.e., image resolution of the target) is normalized with the largest FWHM obtained with the lowest value of $g = 0.51$ to compare the sensitivity to g under different system configurations. The relative enhancement of image resolution of the embedded target provides information on the level of unwanted diffuse light removal.

high anisotropic properties with $g = 0.85$ – 0.9 . As this trend is observed, whether utilizing collimated or diffuse light illumination, it can also relax the requirement of highly

collimated directional illumination onto samples, thus tolerating diffuse light illumination. Therefore, a telecentric lens can provide a simple, yet effective removal of diffuse light in tissue imaging, along with other advantages, such as constant perspective across a large transverse field of view, constant magnification over a long axial field of view, and long working distance between the lens and the sample. We further envision that telecentric lenses could potentially be combined with other types of optical imaging modalities to provide for portable imaging systems, where simple and compact instrumentation design is preferred for diffuse light removal.

Funding. SAMSUNG Global Research Outreach (GRO) Program.

REFERENCES

- Q. Z. Wang, X. Liang, L. Wang, P. P. Ho, and R. R. Alfano, *Opt. Lett.* **20**, 1498 (1995).
- E. Berrocal, D. L. Sedarsky, M. E. Paciaroni, I. V. Meglinski, and M. A. Linne, *Opt. Express* **15**, 10649 (2007).
- W. Cheong, S. A. Prahl, and A. J. Welch, *IEEE J. Quantum Electron.* **26**, 2166 (1990).
- S. L. Jacques, *Phys. Med. Biol.* **58**, R37 (2013).
- R. Samatham, K. G. Phillips, and S. L. Jacques, *J. Innovative Opt. Health Sci.* **3**, 183 (2010).
- Z. Xu, J. Liu, and Y. L. Kim, *J. Biomed. Opt.* **14**, 030510 (2009).
- Z. Xu, J. Liu, D. H. Hong, V. Q. Nguyen, M. R. Kim, S. I. Mohammed, and Y. L. Kim, *IEEE J. Sel. Top. Quantum Electron.* **16**, 815 (2010).
- Z. Xu, A. K. Somani, and Y. L. Kim, *J. Biomed. Opt.* **17**, 0905011 (2012).
- M. Watanabe and S. K. Nayar, *IEEE Trans. Pattern Anal. Mach. Intell.* **19**, 1360 (1997).
- Z. Hu and A. Rollins, *Opt. Express* **13**, 6407 (2005).
- H. S. Sakhalkar and M. Oldham, *Med. Phys.* **35**, 101 (2008).
- A. Thomas, J. Bowsher, J. Roper, T. Oliver, M. Dewhurst, and M. Oldham, *Phys. Med. Biol.* **55**, 3947 (2010).
- A. Thomas, J. Newton, and M. Oldham, *Phys. Med. Biol.* **56**, 4433 (2011).
- A. Tao, Y. Shao, J. Zhong, H. Jiang, M. Shen, and J. Wang, *Biomed. Opt. Express* **4**, 1031 (2013).
- A. Jóźwik, D. Siedlecki, and M. Zając, *Optik* **125**, 6021 (2014).
- R. P. McNabb, P. Challa, A. N. Kuo, and J. A. Izatt, *Biomed. Opt. Express* **6**, 1376 (2015).
- A. Doblas, E. Sanchez-Ortega, M. Martinez-Corral, G. Saavedra, and J. Garcia-Sucerquia, *J. Biomed. Opt.* **19**, 046022 (2014).
- R. L. Konger, Z. Xu, R. P. Sahu, B. M. Rashid, S. R. Mehta, D. R. Mohamed, S. C. DaSilva-Arnold, J. R. Bradish, S. J. Warren, and Y. L. Kim, *Cancer Res.* **73**, 150 (2013).
- S. A. Prahl, M. J. C. V. Gemert, and A. J. Welch, *Appl. Opt.* **32**, 559 (1993).
- A. P. Tzannes and J. M. Mooney, *Opt. Eng.* **34**, 1808 (1995).
- H. C. V. D. Hulst, *Light Scattering by Small Particles* (Courier Corporation, 1957).
- Y. L. Kim, Y. Liu, R. K. Wali, H. K. Roy, M. J. Goldberg, A. K. Kromin, K. Chen, and V. Backman, *IEEE J. Sel. Top. Quantum Electron.* **9**, 243 (2003).
- R. Samatham, S. L. Jacques, and P. Campagnola, *J. Biomed. Opt.* **13**, 041309 (2008).